



Phenotype changes of subchondral plate osteoblasts based on a rat model of ovariectomy-induced osteoarthritis

Ai Jiang^{1#}, Shan Gao^{1#}, Zhenda Zhao¹, Qizhao Tan¹, Shang Sun¹, Chunli Song^{1,2}, Huijie Leng¹

¹Department of Orthopaedics, Peking University Third Hospital, Beijing 100191, China; ²Beijing Key Lab of Spine Diseases, Beijing 100191, China
Contributions: (I) Conception and design: H Leng, A Jiang, S Gao; (II) Administrative support: H Leng; (III) Provision of study materials: A Jiang, Z Zhao, Q Tan, S Sun; (IV) Collection and assembly of data: A Jiang, S Gao, Q Tan; (V) Data analysis and interpretation: A Jiang, S Gao, C Song; (VI) Manuscript writing: All authors; (VII) Final approval of manuscript: All authors.

[#]The authors contributed equally to this work.

Correspondence to: Huijie Leng, Department of Orthopaedics, Peking University Third Hospital, Beijing 100191, China. Email: lenghj@bjmu.edu.cn.

Background: Osteoarthritis (OA) is prevalent in postmenopausal women. Subchondral bone in ovariectomized (OVX) rats might play a more important role in cartilage degeneration compared with other types of OA. How subchondral osteoblast changes in OVX rats is still unclear. Understanding of osteoblast changes obtained from OVX subchondral bone might be helpful to clarify pathogenesis of OVX-OA.

Methods: Female Sprague-Dawley rats were randomly divided into two groups: Sham (n=20) and OVX (n=20). Serum levels of Alkaline phosphatase (ALP) and C-telopeptide of type I collagen (CTX-I) were measured every one or two weeks. All rats were executed at week 9 post surgery. The weight of rats and the wet weight of uterus were assessed. Micro-computed Tomography (micro-CT) was used to analyze the knee microstructure, and toluidine blue staining was employed to evaluate cartilage erosion. Subchondral osteoblast proliferation ability by cell counting kit-8 assay, osteogenic genes expressions by reverse transcription polymerase chain reaction (RT-PCR), differentiation and mineralization ability by ALP staining and alizarin red staining were evaluated and compared between Sham and OVX.

Results: Ovariectomy induced significant increases of serum ALP and CTX-I as early as at week 2. At week 9 after surgery, the body weight of OVX rats was significantly increased, and uterus weight of OVX rats was remarkably decreased. OVX rats demonstrated significant subchondral bone change and cartilage erosion compared with Sham rats. mRNA levels of early markers of osteogenic differentiation (ALP, type I collagen, Runx2) were enhanced in OVX rats, but the late marker (osteocalcin) was not significantly different. ALP activity of osteoblasts increased, but the mineralization capacity decreased in OVX rats.

Conclusions: Subchondral osteoblasts in OVX rats exhibited different proliferation, differentiation and mineralization abilities from normal counterparts.

Keywords: Osteoarthritis (OA); osteoblasts; ovariectomy; phenotype; subchondral bone

Submitted Dec 06, 2019. Accepted for publication Feb 26, 2020.

doi: 10.21037/atm.2020.03.93

View this article at: <http://dx.doi.org/10.21037/atm.2020.03.93>

Introduction

Osteoarthritis (OA) is a common skeletal disease worldwide, especially for the elderly (1). Although OA is mainly characterized by cartilage damage, more and more evidences were acknowledged about the effects of subchondral bone on knee OA (2). However, the exact role

of subchondral bone in cartilage degeneration is unclear. The correlations between cartilage and subchondral bone changes were different among several animal OA models (3), partly because that the role of subchondral bone might depend on specific OA pathologies (estrogen deficiency, trauma or aging) and specific phase of OA progression (4).

OA is more prevalent in postmenopausal women than age-matched men, implying a link between estrogen and OA (5). Estrogen deficiency is well known for accelerating bone loss (6), while its relation to OA is still uncertain. Most studies investigating the role of subchondral bone in OA adopted the post traumatic osteoarthritis (PT-OA) models which induced cartilage abrasion rapidly by creating instant mechanical instability of joints, such as anterior cruciate ligament transection (ACLT) (7). Those models provided important information about subchondral bone remodeling for PT-OA (8), but they are hardly able to simulate estrogen deficiency induced OA and target very early stage of cartilage degeneration in postmenopausal OA. The mild erosion at the very early stage of OA is repairable and the early stage of OA might be a promising therapeutic window for reversing the progression of OA (9,10). Ovariectomy induced OA (OVX-OA) was developed to simulate postmenopausal OA and validated to better present the very early stage of OA (11).

How subchondral osteoblast changes under estrogen deficiency induced OA is a significant problem. Clinical and experimental studies have already demonstrated that the structural and functional integrity of articular cartilage depend on well-balanced subchondral bone turnover (12). Bone turnover is a delicately regulated process involving osteoblasts-related bone formation and osteoclast-related bone resorption (13). Osteoclast-mediated bone resorption can be regulated by osteoblasts, which secrete cytokines essential for osteoclast formation, such as receptor activator of nuclear factor κ B ligand (RANKL) (14) and osteoprotegerin (OPG) (15), indicating that osteoblasts might play an indispensable role in osteoclast function. Based on osteoblasts' important role in bone turnover, this study focused on phenotype changes of osteoblasts.

Rat OVX-OA model was developed, and 9-week post-surgery was validated to be long enough to induce significant cartilage erosion (11), while subchondral osteoblast changes in OVX-OA rats have yet been investigated. Considering the special role of osteoblasts in bone remodeling, we speculated that phenotype changes of osteoblasts might be closely related to the development of OVX-OA. A better understanding of osteoblast phenotype in rat OVX-OA model could broaden our knowledge with respect to the contribution of subchondral bone to cartilage degradation and their possibility as a therapeutic target for

postmenopausal OA.

Methods

Animals

A total of 40 six-month-old female Sprague-Dawley (SD) rats were purchased from the Department of Laboratory Animal Science of Peking University Health Science Center (Beijing, China). The rats were raised 2 or 3 per cage at 25 °C with a 12 h light/dark cycle, and they were provided with water or food *ad libitum*. The rats were acclimatized to the laboratory environment for at least one week before surgery.

All rats were weighted before surgery. Randomly selected 20 rats were subjected to bilateral ovariectomy. The remaining rats underwent sham operation (Sham) simply exposing the ovaries. At week 9 after surgery, all the rats were weighted again before execution. After euthanasia, uterus and knee joint samples from both OVX and Sham rats were collected for follow-up studies.

Blood sample collection

Animals were fasted for more than 12 hours before sampling. The blood samples were collected at week 0 (baseline), 2, 3, 5, 7 and 9 after surgery respectively. Blood samples were centrifuged at 4 °C and stored at -80 °C for later use. Commercial enzyme-linked immunosorbent assay (ELISA) kits were used to evaluate serum levels of alkaline phosphatase (ALP; BioVision, Milpitas, CA, USA) and C-telopeptide of type I collagen (CTX-I; Novus Biologicals, Littleton, CO).

Micro-CT analysis

After sacrifice, knee joints were collected. Adhering soft tissues such as skin and muscles were removed. The specimens were fixed in 4% paraformaldehyde (Solarbio, Beijing, China). The tibia parts of the joints were scanned with 500 μ A current, 80 kV voltage, 360° rotation angle, 360 rotation steps and reconstructed with 13 μ m resolution by micro-CT (Inveon, Siemens, USA). The scanned data were imported into the Inveon Research Workplace (Siemens, USA) for image analysis. Quantification of bone

volume fraction (BV/TV) was analyzed.

Histological assessment

The samples were fixed using paraformaldehyde, and decalcified for at least 2 weeks in 10% EDTA solution (Zsjiqbio, Beijing, China). The decalcified samples were embedded in paraffin wax and cut into four-micrometer-thick sections. These sections were subjected to toluidine blue staining (Solarbio) to evaluate the structural integrity of cartilage. Briefly, knee sections were incubated in 1% toluidine blue solution for 30 min, and then pictures were collected for further analysis. The erosion length and total length of cartilage surface were calculated based on the stained slices by Image-Pro Plus software (Version 6.0, Media Cybernetics, USA). The severity score was quantified as the ratio of the length of the damaged area to the total length of the cartilage surface.

Isolation and culture of subchondral osteoblasts

All the following operations were performed under aseptic conditions. The cartilage layer and subchondral trabecular bone were carefully removed under magnifying microscope. The remaining subchondral bone plate was dissected into separate bone chips, which were then incubated in 1% trypsin (Gibco, CA, USA) in a humidified environment containing 5% CO₂ at 37 °C for 10 min. Then the trypsin solution was replaced with 0.2% collagenase solution (Invitrogen, Carlsbad, CA, USA) (16). After incubation for 30 min, the bone chips were transferred to a 75 cm² culture flask and cultivated in alpha-Minimal Eagle Medium (αMEM; Gibco) replenished with 20% fetal bovine serum (FBS; Gibco), 100 units/mL penicillin (HyClone, Logan, UT, USA) and 100 µg/mL streptomycin (HyClone). The medium was changed every 2 or 3 days. When cells were observed in 75 cm² culture flask, fresh medium containing 10% FBS was utilized. Primary osteoblasts were digested and passaged when cells reached 80% to 90% confluence. Only osteoblasts in passage 1 were used in our following experiments.

Cell viability assay

Cell counting kit-8 (CCK8) assay was performed to evaluate the viability of osteoblasts. Osteoblasts were plated in 96-well plates at a density of 5×10³ cells per well. After 24, 48 and 72 h respectively, 10:l CCK-8 solution (Dojindo,

Kumamoto, Japan) was added into each well and the plates were incubated at 37 °C for 2 hours. The absorbance value of each well was detected by a microplate reader (Thermo Fisher Scientific, Waltham, MA, USA) at 450 nm wave length.

Immunofluorescence staining

Osteoblasts were fixed with 4% paraformaldehyde for 30 min and permeabilized with 0.2% Triton X-100 (Beyotime Biotechnology, Beijing, China) for 5 min at room temperature. Osteoblasts were blocked with goat serum for 1 h, and incubated in primary antibody against type I collagen (Abcam, Cambridge, MA, USA; 1:200) at 4 °C overnight. Followed by PBS washing, incubation with second antibody (Abcam; 1:200) was conducted for 1 h at room temperature. The nuclei of cells were counterstained by DAPI solution (Solarbio) and images were captured using fluorescence microscopy (Nikon, Tokyo, Japan).

RNA extraction and RT-PCR

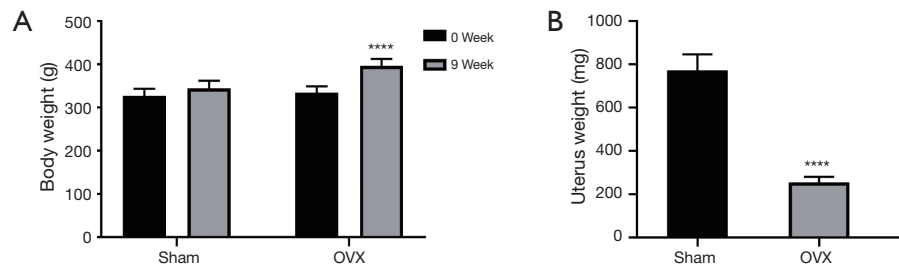
Osteoblasts were treated with osteogenic medium containing 50 µg/mL ascorbate, 2 mM β-glycerophosphate and 10 nM dexamethasone (Sigma-Aldrich, St. Louis, MO, USA) for 7 days, and then total RNA was extracted using TRIzol (Invitrogen). The concentration and purity of RNA were measured by Nanodrop 2000C (Thermo Fisher). 1 µg RNA was used for reverse transcription with a final reaction volume of 20 µL using RevertAid First Strand cDNA Synthesis Kits (Thermo Fisher). Real-time reverse transcription polymerase chain reaction (RT-PCR) was carried out employing the Step-One-Plus Real-time PCR System (Applied Biosystems, Foster City, CA, USA). Relative transcription levels of osteogenic genes, such as ALP, type I collagen (Col-I), osteocalcin (OCN) and runt-related transcription factor 2 (Runx2), calculated by 2^{-ΔΔCT} method (17), were normalized to the values from Sham group with glyceraldehyde-3-phosphate dehydrogenase (GAPDH) as the housekeeping gene. The primer sequences of osteogenic genes are shown in *Table 1*.

ALP staining and activity assay

Osteoblasts were seeded in 12-well plates at a density of 5×10⁴ cells/well in osteogenic medium for 7 days. ALP staining of osteoblasts were conducted using a commercial staining kit (Beyotime Biotechnology). In brief, osteoblasts

Table 1 Primer sequences of osteogenic genes

Genes	Sense	Antisense
<i>GAPDH</i>	GCAAGTTCAACGGCACAG	GCCAGTAGACTCCACGACA
<i>Col-1</i>	GCAATGCTGAATCGTCCCAC	CAGCACAGGCCCTCAAAAAC
<i>ALP</i>	CCTTGAAAAATGCCCTGAAA	CTTGAGAGAGCCACAAAGG
<i>OCN</i>	CCGTTTAGGGCATGTGTTGC	CCGTCCATACTTTCGAGGCA
<i>Runx2</i>	GAGCACAAACATGGCTGAGA	TGGAGATGTTGCTCTGTTCC

**Figure 1** Body weight (A) and uterus weight (B) of all rats. n=20 for each group; ****, $P < 0.0001$.

were fixed with 4% paraformaldehyde and gently washed with PBS, after which they were stained with NBT/BCIP staining solution at room temperature for 30 min in dark conditions. Representative images were acquired for follow-up comparison.

In ALP activity assay, 1% triton-X was added to lyse osteoblasts, and the supernatant was collected (18). The relative activity of ALP was analyzed using p-nitrophenyl phosphate (pNPP; Beyotime) as the substrate. The mixture of supernatant and pNPP was incubated at 37 °C for 30 min on a bench shaker and the reaction was stopped by 20 nM NaOH (Sigma-Aldrich). The absorbance was measured at 405 nm using a microplate reader (Thermo Fisher). Finally, ALP activity was normalized by total protein concentration measured by a BCA protein assay kit (Beyotime Biotechnology).

Mineralization analysis

Mineralization assays of osteoblasts were performed in 12-well plates using Alizarin red S staining kits (VivaCell, Shanghai, China). The cells were treated with osteogenic medium for 14 d. After washing with PBS three times, osteoblasts were fixed with 4% paraformaldehyde at room temperature for 15 min, and then stained with 0.2% Alizarin Red-S at 37 °C for 1 h (19). The semi quantification

of Alizarin Red S staining was performed utilizing 1% cetylpyridinium chloride extraction (Sigma), followed by measurement using a microplate reader (Thermo Fisher) at 550 nm (20).

Statistical analysis

All data were expressed as mean \pm standard deviation (SD), and data analysis was conducted using SPSS 24.0 software (SPSS, Chicago, USA). Statistical differences were calculated utilizing two-tailed unpaired Student's *t*-test (one variant, two groups), or two-way ANOVA (two or more variants, two groups). *P* values less than 0.05 was considered as statistically different.

Results

Body weight and wet weight of the uterus

Weights of body and wet uterus are shown in *Figure 1* (n=20 for each group). There was no statistical difference in body weights between Sham and OVX groups at week 0 (*Figure 1A*). The body weight of Sham group at week 9 was not statistically different compared with that at week 0. The body weight of OVX group at week 9 increased significantly in comparison with the baseline (week 0). There was a

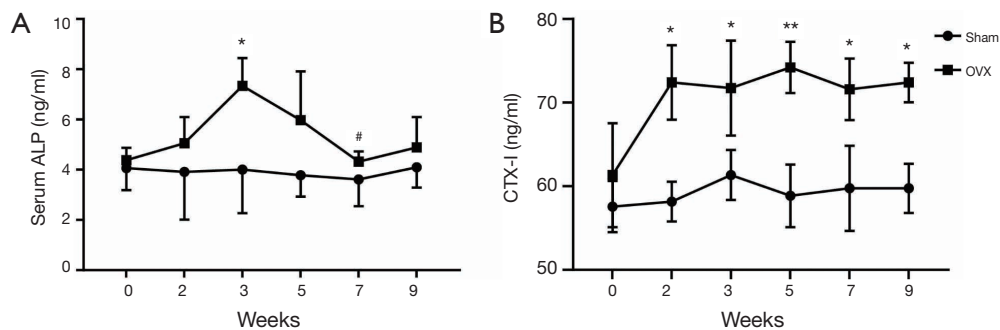


Figure 2 Changes of serum alkaline phosphatase (ALP) (A) and C-telopeptide of type I collagen (CTX-I) (B) in OVX and Sham groups. n=6 for each group; *, P<0.05 compared with OVX group at week 0; **, P<0.01 compared with OVX group at week 0; #, P<0.05 compared with OVX group at week 3.

dramatic loss of uterine weight of OVX group compared with Sham group at week 9 (*Figure 1B*).

Changes in serum parameters

The variation tendency of serum ALP and CTX-I in Sham and OVX groups are shown in *Figure 2* (n=6 for each group). The serum ALP concentration of Sham group was relatively steady. OVX group experienced oscillation of ALP concentration and reached the peak value at week 3 (*Figure 2A*). Compared with sham operation, OVX significantly enhanced CTX-I expression since week 2 (*Figure 2B*).

Subchondral bone microstructure changes

Alterations in subchondral bone microstructure were examined at week 9 post surgery (n=5). The subchondral bone in OVX group experienced more bone loss than that in Sham group, and large areas of bone marrow could be observed in micro-CT images (*Figure 3A,B*). Quantitative results confirmed that the bone volume fraction (BV/TV) of OVX group was significantly lower than that of Sham group (*Figure 3C*).

Cartilage erosion

Surface erosion of articular cartilage was assessed based on toluidine blue staining (n=5). Toluidine blue is a cationic dye that can combine with proteoglycan specifically. Sham group presented smooth articular cartilage surface (*Figure 3D*), while OVX group displayed that mild erosion appeared on the cartilage surface as shown by the black arrow (*Figure 3E*). The quantification result illustrated

significant difference of cartilage surface erosion between OVX and Sham groups (*Figure 3F*).

Cell viability assay

An upward trend of both groups (n=6) was observed over time (*Figure 4A*). Osteoblast viability of OVX group was significantly higher than that of Sham group at 24, 48, 72 h respectively (P<0.05).

Immunofluorescence staining

Fluorescence images revealed that Col-I content (green) was significantly increased in OVX group (*Figure 4B*, n=6 for each group). Quantitative analysis of immunofluorescence intensity was displayed in *Figure 4C*.

Relative expression of osteogenic genes

Osteogenic genes, which were associated with osteoblast differentiation and mineralization, were studied using real-time RT-PCR (n=6). Osteoblasts were induced using osteogenic medium for 7 d, and mRNA levels were compared at the termination of the experiment. Osteogenesis differentiation markers, including ALP, Col-I and Runx2, were significantly higher in OVX osteoblasts than age-matched Sham ones (P<0.05, *Figure 5*). There was no significant difference concerning the expression level of OCN (P>0.05, *Figure 5*).

ALP staining and activity assay (*Figure 6*)

ALP was an important marker with respect to osteoblast

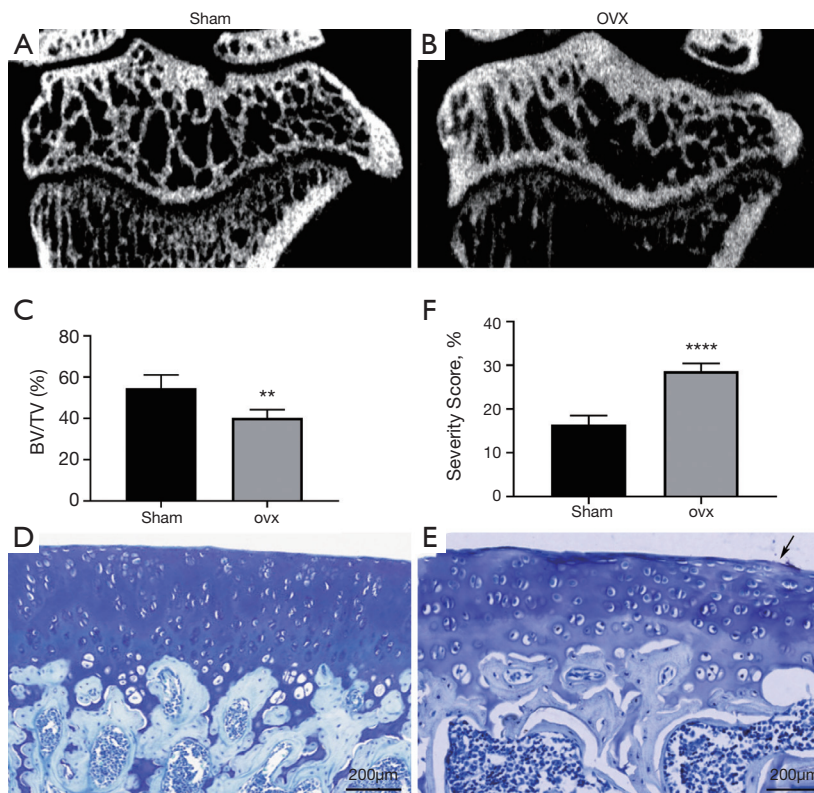


Figure 3 Comparisons of articular cartilage and subchondral bone between Sham and OVX rats at week 9: subchondral bone microstructure in Sham group (A) and OVX group (B) with the quantification results of micro-CT analysis (C); cartilage erosion in Sham group (D, scale bar =200 μ m) and OVX group (E, scale bar =200 μ m) with the quantification of severity scores (F). The black arrow points to the surface erosion of articular cartilage (E). n=5 for each group; **, $P<0.01$; ****, $P<0.0001$ vs. Sham group; BV/TV, bone volume fraction.

differentiation. ALP staining of OVX group (Figure 6B) was enhanced compared with Sham group (Figure 6A). Further quantification using ALP activity assay demonstrated that the difference between OVX and Sham groups was statistically significant (Figure 6E, n=6).

Mineralization analysis (Figure 6)

Calcium nodule deposition was observed after osteoblasts were induced for 12 d (not shown). The number and area of mineralized nodules in Sham group (Figure 6C) were greater than that in OVX group (Figure 6D) after induction for 14 d, indicating OVX osteoblasts were less effective in inducing calcium nodule formation ($P<0.05$, n=6 for each group). The semiquantitative analysis of Alizarin Red-S staining revealed that mineralization capacity of OVX group was significantly lower than that of Sham group (Figure 6F).

Discussion

The present study used the rat OVX-OA model to simulate the very early stage of estrogen deficiency induced OA occurring in postmenopausal women (11). Clinical techniques are unable to detect symptoms for the very early stage of human OA. The clinical samples collected from late-stage OA patients can not accurately reflect the early changes in bone and cartilage (21), making it necessary to employ animal models of early OA. Animal studies demonstrated that early OA were successfully constructed in rats by OVX at week 9 and the cartilage erosion could be recovered by appropriate treatments (22,23). The model was confirmed by rat body weight, uterine weight (Figure 1), serum levels of bone metabolism markers (Figure 2) and cartilage surface erosion (Figure 3).

Procedure of cartilage degeneration was divided into two stages based on clinical observation. At the early stage,

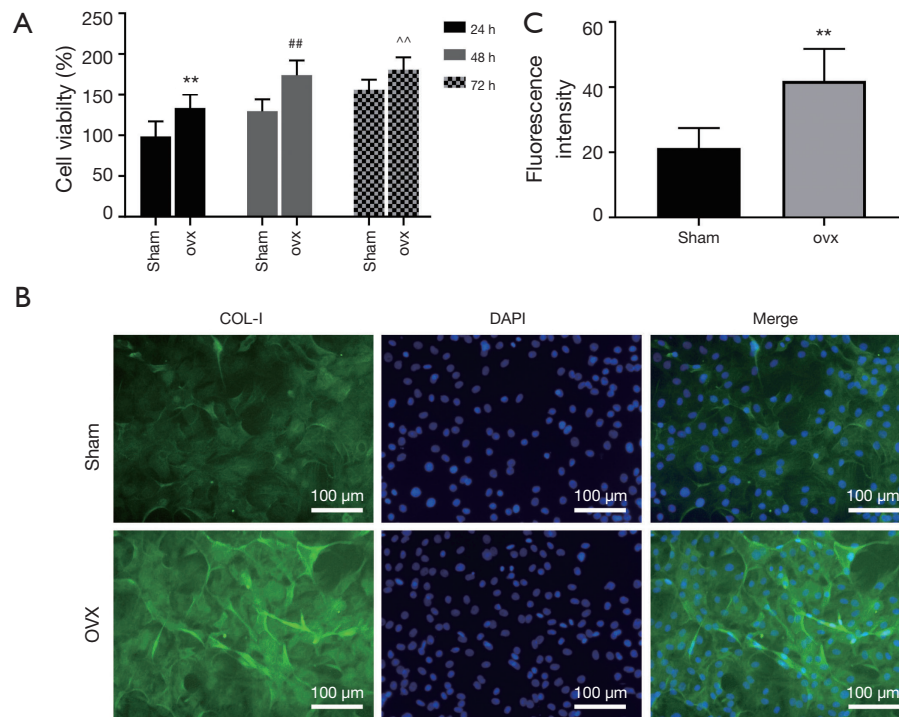


Figure 4 Osteoblast viabilities in Sham and OVX groups detected at indicated time using CCK8 kits (A). $n=6$ for each group; **, $P<0.01$ compared with Sham group after 24-hour culture; ##, $P<0.01$ compared with Sham group after 48-hour culture; ^^, $P<0.01$ compared with Sham group after 72-hour culture. Immunofluorescence staining for Col-I in primary osteoblasts derived from Sham and OVX rats (B; $n=6$; scale bar =100 μm) and quantification of fluorescence intensity (C); **, $P<0.01$.

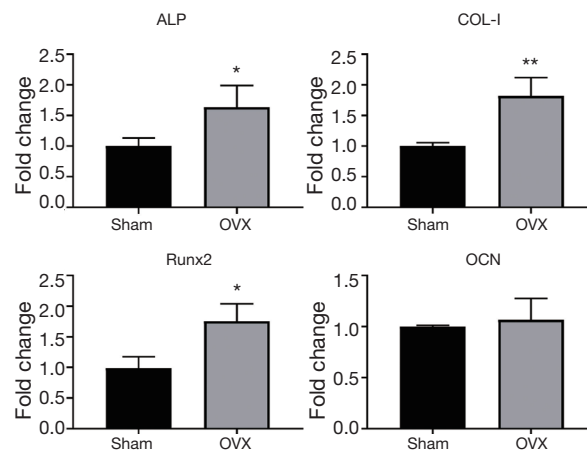


Figure 5 Relative expression of mRNA levels for ALP, Col-I, Runx2 and OCN in osteoblasts obtained from Sham and OVX rats. Data were expressed as fold change over Sham. $n=6$; *, $P<0.05$; **, $P<0.01$ vs. Sham. ALP, alkaline phosphatase; Col-I, type I collage; Runx2, runt related transcription factor 2; OCN, osteocalcin.

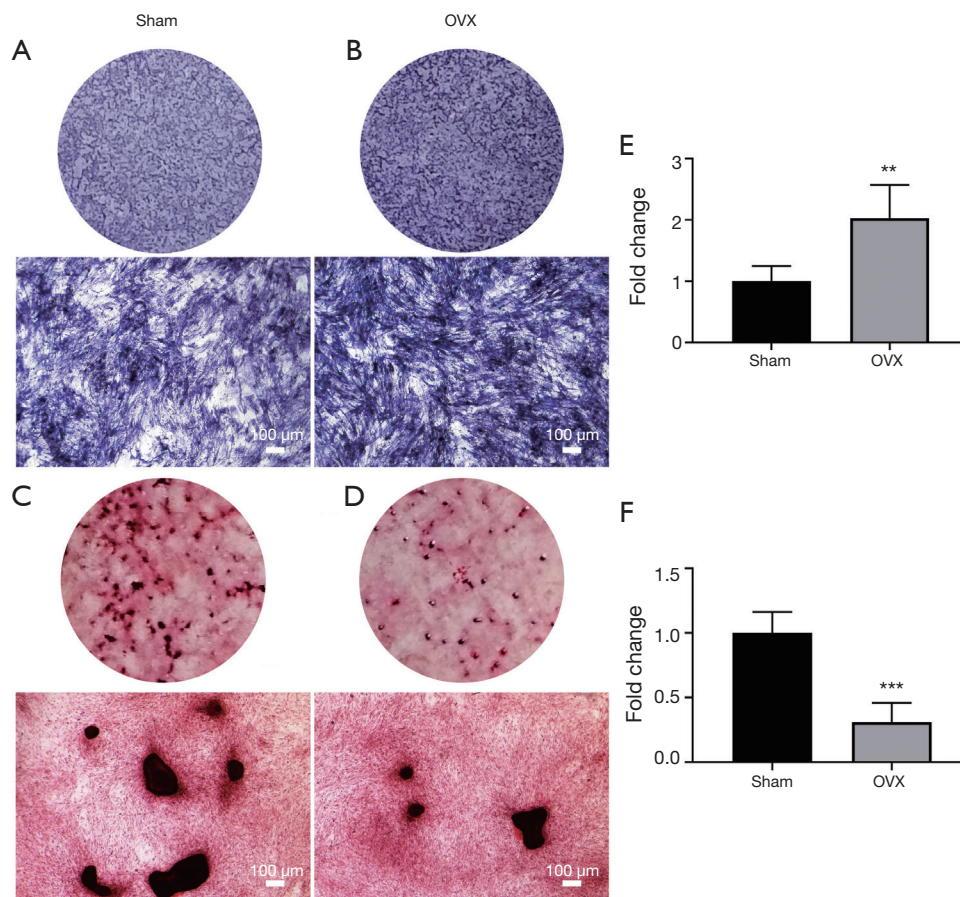


Figure 6 Comparison of ALP activity and mineralization ability of osteoblasts between Sham (A,C) and OVX (B,D) groups. Representative images of ALP staining at day 7 after osteogenic induction of both groups (A,B). The ALP activity assays showed fold changes over Sham (E). Representative images of Alizarin red S staining at day 14 after osteoinduction of both groups (C,D). The semiquantitative results of calcium nodule staining are displayed in (F). n=6 for each group; **, P<0.01 compared with Sham group; ***, P<0.001 by comparison to Sham group; scale bar =100 μ m.

lesions occurred on the cartilage surface, while they extended into deep layers at the late stage (24). The present study showed that OVX-OA model resulted in proteoglycan loss, with mild erosion appeared only at the peripheral regions of cartilage at week 9 (Figure 3), indicating that cartilage degeneration in this model was relatively mild, and even earlier than the defined 'early stage' of OA in clinics (25). There might exist a 'very-early' stage of cartilage degeneration. This very-early stage might be repairable and crucial for cartilage regeneration. A prior study revealed that if proteoglycan integrity is preserved in the early stages of the disease, irreversible cartilage defects can be prevented (26). Therefore, intervention and treatment in the early stage of the disease are of great significance for reversing OA progress (10).

The phenotype changes of subchondral osteoblasts after ovariectomy was investigated in this study. Changes of osteoblasts were demonstrated as altered proliferation, differentiation and mineralization capacities. Based on the results, the phenotype of osteoblasts in OVX-OA rats was different from that of normal cells. Other studies based on OA patients also showed that osteoblasts from subchondral bone presented different phenotypes and gene expressions compared with normal subjects (27,28). The viability of subchondral osteoblasts at week 9 after OVX was higher than that of Sham group (Figure 4), which could be attributed to the increased systemic factors in response to estrogen deficiency during early estrogen withdrawal (29). However, a study in osteoporotic patients (76.0 \pm 5.6 yr) reported that proliferation activity of osteoblasts was lower

than normal counterparts (30). It is worth noting that the above research studied elderly women who suffered severe osteoporosis and selected osteoblasts from subchondral trabecular bone to investigate, which might result in the discrepant results between our study. It seems that osteoblasts might display different proliferation capacity at different stages of the disease and at different anatomical locations.

Our results demonstrated that the relative expression of early osteogenic genes including ALP, Col-I, Runx2 was enhanced in OVX group (*Figure 5*) with elevated proliferation ability of osteoblasts. This finding is consistent with Neve's observation that osteoblast progenitors could promote the expression of several genes encoding for bone-specific matrix composition, such as Col-I, during active proliferation period (31). ALP is one of the early markers of osteogenic differentiation. Runx2 is a crucial transcription factor playing a critical role in the early osteoblastogenesis (32). Runx2 is also involved in the up-regulation of other osteogenic genes such as Col-I (33) and OCN (34). Meanwhile, ALP, Col-I and OCN can also enhance Runx2 expression (35,36). All of these genes are closely related and interacted. In this study, the expressions of ALP, Col-I and Runx2 were all elevated in OVX osteoblasts, whereas the mRNA level of OCN, a late differentiation marker, showed no statistical difference among two cohorts (*Figure 5*), which might be ascribed to the duration of osteogenetic induction. In the present research, osteoblasts were induced using osteogenetic medium only for 7 d. Borzos's study showed that it took at least 21 days to induce an increase in OCN expression (37). OCN is indispensable for the mineral deposition and osteoblast differentiation as a matrix signaling molecule, and is treated as an indicator of mature osteoblasts (38).

In skeleton, ALP is mainly expressed on the surface of osteoblasts, and is commonly used as a biomarker for osteoblasts due to its critical role in matrix formation and mineralization (6). Results of ALP staining and activity assays demonstrated that OVX could increase the activity of ALP in osteoblasts (*Figure 6*), partly due to high subchondral bone turnover induced by OVX. Bone turnover can be reflected by serum markers of bone formation and bone resorption (39). Both ALP, a marker of bone formation, and CTX-I, a marker of bone resorption, were increased after OVX (*Figure 2*), suggesting high bone turnover in OVX rats. Increased bone turnover in OVX group was further verified from micro-CT analysis (*Figure 3*). A previous study also showed a significant increase in subchondral ALP expression on rats at 38 d after OVX (40). Another study found lower ALP expression after

OVX (13), probably because that study focused on ALP expression in the tissue on the protein level and used rats at 22 weeks after OVX.

Mineralization of bone matrix is an important part of osteoblast maturation. Alizarin red S staining can detect calcium deposition of extracellular matrix (41). After induction for 14 d, formation of calcium nodules in OVX group was significantly reduced, suggesting a decreased mineralization ability of OVX osteoblasts (*Figure 6*). The decreased mineralization is consistent with bone loss and microstructural change shown by micro-CT analysis. It might also be responsible for formation of excessive osteoid that could not mineralize normally in vivo, which was an important pathologic change in OA (42). In the present study, OVX-OA osteoblasts produced more Col-I than Sham ones as demonstrated by fluorescence staining and RT-PCR. Some researches revealed that OA osteoblasts produced more Col-I than normal counterparts, but with a changed ratio of $\alpha 1$ to $\alpha 2$ chains, especially with a rise of the $\alpha 1$ chain, thus resulting in the aberrant mineralization (43). The increase of early osteogenic markers (ALP, Col-I and Runx-2), but decline of mineralization capacity implied osteoblasts could only progress into a certain point and could not completely differentiate into mature osteoblasts producing mineralized matrix (43).

There are several limitations for the current study which are worth mentioning. First, this study used the osteoblasts from rats. Isolation and culture of the cells might have effects on the phenotype changes of osteoblasts. To minimize phenotype changes of osteoblasts due to techniques for cell isolation and culture, only primary osteoblasts in passage 1 were used. Moreover, Sham group was designed whose cells also experienced the same procedure as OVX group, and the results might best diminish the effects of those techniques and just show the effects of OVX by comparing OVX group with Sham group. In the future, when the effects of isolation and culture of cells on osteoblast changes are stressed, immunohistology analysis might be desirable. Secondly, this study aimed to illustrate osteogenesis related phenotype changes of osteoblast in subchondral bone at the early stage of OVX-OA, including proliferation, extracellular matrix synthesis, and mineralization. However, other aspects of osteoblasts, such as migration capacity, apoptosis related genes' expression, changes at different time points after OVX, and even the crosstalk with chondrocytes which would help further clarify the role of osteoblasts in OA, might also be important to reveal comprehensive changes

of osteoblasts and provide hints on related mechanisms. Information of all those aspects will be valuable for better understanding the exhaustive details of osteoblast changes.

Conclusions

In the rat OVX-OA, subchondral osteoblasts exhibited different phenotypes from normal counterparts. A better understanding of osteogenetic phenotypes of OVX-OA osteoblasts could provide new insight into the contribution of osteoblasts to cartilage degradation and their feasibility as a therapy target for postmenopausal OA.

Acknowledgments

Funding: This work was supported by the National Natural Science Foundation of China [grant numbers 11872076, 11472017].

Footnote

Conflicts of Interest: All authors have completed the ICMJE uniform disclosure form (available at <http://dx.doi.org/10.21037/atm.2020.03.93>). The authors have no conflicts of interest to declare.

Ethical Statement: The authors are accountable for all aspects of the work in ensuring that questions related to the accuracy or integrity of any part of the work are appropriately investigated and resolved. All animal experiments were approved by the Peking University Animal Ethics Committee (permission number: LA2019209), and were implemented complying with the Guidelines for the Care and Use of Laboratory Animals.

Open Access Statement: This is an Open Access article distributed in accordance with the Creative Commons Attribution-NonCommercial-NoDerivs 4.0 International License (CC BY-NC-ND 4.0), which permits the non-commercial replication and distribution of the article with the strict proviso that no changes or edits are made and the original work is properly cited (including links to both the formal publication through the relevant DOI and the license). See: <https://creativecommons.org/licenses/by-nc-nd/4.0/>.

References

1. Tong C, Liang H, Liu X, et al. The protective effects of exenatide against AGEs-induced articular matrix degradation in human primary chondrocytes. *Am J Transl Res* 2019;11:2081-9.
2. Hügle T, Geurts J. What drives osteoarthritis?-synovial versus subchondral bone pathology. *Rheumatology (Oxford)* 2017;56:1461-71.
3. Kuyinu EL, Narayanan G, Nair LS, et al. Animal models of osteoarthritis: classification, update, and measurement of outcomes. *J Orthop Surg Res* 2016;11:19.
4. Karsdal MA, Bay-Jensen AC, Lories RJ, et al. The coupling of bone and cartilage turnover in osteoarthritis: opportunities for bone antiresorptives and anabolics as potential treatments? *Ann Rheum Dis* 2014;73:336-48.
5. Watt FE. Hand osteoarthritis, menopause and menopausal hormone therapy. *Maturitas* 2016;83:13-8.
6. Chung HJ, Kim WK, Oh J, et al. Anti-Osteoporotic Activity of Harpagoside by Upregulation of the BMP2 and Wnt Signaling Pathways in Osteoblasts and Suppression of Differentiation in Osteoclasts. *J Nat Prod* 2017;80:434-42.
7. Aizah N, Chong PP, Kamarul T. Early Alterations of Subchondral Bone in the Rat Anterior Cruciate Ligament Transection Model of Osteoarthritis. *Cartilage* 2019;1947603519878479. [Epub ahead of print].
8. Maerz T, Kurdziel M, Newton MD, et al. Subchondral and epiphyseal bone remodeling following surgical transection and noninvasive rupture of the anterior cruciate ligament as models of post-traumatic osteoarthritis. *Osteoarthritis and Cartilage* 2016;24:698-708.
9. Parazzini F. Menopausal status, hormone replacement therapy use and risk of self-reported physician-diagnosed osteoarthritis in women attending menopause clinics in Italy. *Maturitas* 2003;46:207-12.
10. Bokhari RA, Tantowi N, Lau SF, et al. Java Tea (*Orthosiphon stamineus*) protected against osteoarthritis by mitigating inflammation and cartilage degradation: a preclinical study. *Inflammopharmacology* 2018;26:939-49.
11. Høegh-Andersen P, Tanko LB, Andersen TL, et al. Ovariectomized rats as a model of postmenopausal osteoarthritis: validation and application. *Arthritis Res Ther* 2004;6:R169-80.
12. Hayami T, Pickarski M, Wesolowski GA, et al. The role of subchondral bone remodeling in osteoarthritis: reduction of cartilage degeneration and prevention of osteophyte formation by alendronate in the rat anterior cruciate ligament transection model. *Arthritis Rheum* 2004;50:1193-206.
13. Bellido M, Lugo L, Roman-Blas JA, et al. Subchondral bone microstructural damage by increased remodelling

- aggravates experimental osteoarthritis preceded by osteoporosis. *Arthritis Res Ther* 2010;12:R152.
14. Rahman MM, Bhattacharya A, Fernandes G. Conjugated linoleic acid inhibits osteoclast differentiation of RAW264.7 cells by modulating RANKL signaling. *J Lipid Res* 2006;47:1739-48.
 15. Allison H, McNamara LM. Inhibition of osteoclastogenesis by mechanically stimulated osteoblasts is attenuated during estrogen deficiency. *American journal of physiology Cell physiology* 2019;317:C969-C982.
 16. Perpétuo IP, Bourne LE, Orriss IR. Isolation and Generation of Osteoblasts. *Methods Mol Biol* 2019;1914:21-38.
 17. Yamasaki S, Mera H, Itokazu M, et al. Cartilage Repair With Autologous Bone Marrow Mesenchymal Stem Cell Transplantation: Review of Preclinical and Clinical Studies. *Cartilage* 2014;5:196-202.
 18. Radhakrishnan J, Manigandan A, Chinnaswamy P, et al. Gradient nano-engineered in situ forming composite hydrogel for osteochondral regeneration. *Biomaterials* 2018;162:82-98.
 19. Zhai Y, Li Y, Wang Y, et al. Psoralidin, a prenylated coumestan, as a novel anti-osteoporosis candidate to enhance bone formation of osteoblasts and decrease bone resorption of osteoclasts. *Eur J Pharmacol* 2017;801:62-71.
 20. Son JH, Cho YC, Sung IY, et al. Melatonin promotes osteoblast differentiation and mineralization of MC3T3-E1 cells under hypoxic conditions through activation of PKD/p38 pathways. *J Pineal Res* 2014;57:385-92.
 21. Finnilä MA, Thevenot J, Aho OM, et al. Association between subchondral bone structure and osteoarthritis histopathological grade. *J Orthop Res* 2017;35:785-92.
 22. Oestergaard S, Sondergaard BC, Hoegh-Andersen P, et al. Effects of ovariectomy and estrogen therapy on type II collagen degradation and structural integrity of articular cartilage in rats: implications of the time of initiation. *Arthritis Rheum* 2006;54:2441-51.
 23. Sondergaard B-C, Oestergaard S, Christiansen C, et al. The effect of oral calcitonin on cartilage turnover and surface erosion in an ovariectomized rat model. *Arthritis Rheum* 2007;56:2674-8.
 24. Stoop R, Buma P, van der Kraan PM, et al. Differences in type II collagen degradation between peripheral and central cartilage of rat stifle joints after cranial cruciate ligament transection. *Arthritis Rheum* 2000;43:2121-31.
 25. Lin AC, Seeto BL, Bartoszko JM, et al. Modulating hedgehog signaling can attenuate the severity of osteoarthritis. *Nature Medicine* 2009;15:1421-5.
 26. Pratta MA, Yao W, Decicco C, et al. Aggrecan protects cartilage collagen from proteolytic cleavage. *J Biol Chem* 2003;278:45539-45.
 27. Hilal G, Martel-Pelletier J, Pelletier JP, et al. Osteoblast-like cells from human subchondral osteoarthritic bone demonstrate an altered phenotype in vitro: possible role in subchondral bone sclerosis. *Arthritis Rheum* 1998;41:891-9.
 28. Sakao K, Takahashi KA, Mazda O, et al. Enhanced expression of interleukin-6, matrix metalloproteinase-13, and receptor activator of NF-kappaB ligand in cells derived from osteoarthritic subchondral bone. *J Orthop Sci* 2008;13:202-10.
 29. Yokose S, Ishizuya T, Ikeda T, et al. An estrogen deficiency caused by ovariectomy increases plasma levels of systemic factors that stimulate proliferation and differentiation of osteoblasts in rats. *Endocrinology* 1996;137:469-78.
 30. Perrini S, Natalicchio A, Laviola L, et al. Abnormalities of insulin-like growth factor-I signaling and impaired cell proliferation in osteoblasts from subjects with osteoporosis. *Endocrinology* 2008;149:1302-13.
 31. Neve A, Corrado A, Cantatore FP. Osteoblast physiology in normal and pathological conditions. *Cell Tissue Res* 2011;343:289-302.
 32. Brion A, Zhang G, Dossot M, et al. Nacre extract restores the mineralization capacity of subchondral osteoarthritis osteoblasts. *J Struct Biol* 2015;192:500-9.
 33. Ducy P, Zhang R, Geoffroy V, et al. *Osf2/Cbfa1*: a transcriptional activator of osteoblast differentiation. *Cell* 1997;89:747-54.
 34. Tsai MT, Lin YS, Chen WC, et al. editors. *Runx2 and Osterix gene expression in human bone marrow stromal cells are mediated by far-infrared radiation* 2011.
 35. An J, Yang H, Zhang Q, et al. Natural products for treatment of osteoporosis: The effects and mechanisms on promoting osteoblast-mediated bone formation. *Life Sci* 2016;147:46-58.
 36. Gu Q, Cai Y, Huang C, et al. Curcumin increases rat mesenchymal stem cell osteoblast differentiation but inhibits adipocyte differentiation. *Pharmacogn Mag* 2012;8:202-8.
 37. Gharibi B, Ghuman MS, Cama G, et al. Site-specific differences in osteoblast phenotype, mechanical loading response and estrogen receptor-related gene expression. *Mol Cell Endocrinol* 2018;477:140-7.
 38. Positong S, Hong JM, Eleniste PP, et al. *Pyk2* deficiency potentiates osteoblast differentiation and mineralizing activity in response to estrogen or raloxifene. *Mol Cell*

- Endocrinol 2018;474:35-47.
39. Bahlous A, Kalai E, Hadj Salah M, et al. Biochemical markers of bone remodeling: recent data of their applications in managing postmenopausal osteoporosis. *Tunis Med* 2006;84:751-7.
 40. Mukherjee M, Das AS, Mitra S, et al. Prevention of bone loss by oil extract of garlic (*Allium sativum* Linn.) in an ovariectomized rat model of osteoporosis. *Phytother Res* 2004;18:389-94.
 41. Isama K, Tsuchiya T. Enhancing effect of poly(L-lactide) on the differentiation of mouse osteoblast-like MC3T3-E1 cells. *Biomaterials* 2003;24:3303-9.
 42. Truong LH, Kuliwaba JS, Tsangari H, et al. Differential gene expression of bone anabolic factors and trabecular bone architectural changes in the proximal femoral shaft of primary hip osteoarthritis patients. *Arthritis Res Ther* 2006;8:R188.
 43. Couchourel D, Aubry I, Delalandre A, et al. Altered mineralization of human osteoarthritic osteoblasts is attributable to abnormal type I collagen production. *Arthritis Rheum* 2009;60:1438-50.

Cite this article as: Jiang A, Gao S, Zhao Z, Tan Q, Sun S, Song C, Leng H. Phenotype changes of subchondral plate osteoblasts based on a rat model of ovariectomy-induced osteoarthritis. *Ann Transl Med* 2020;8(7):476. doi: 10.21037/atm.2020.03.93